



# INFLUENCE OF THE DEPTH OF EMBEDMENT ON SEISMIC EARTH PRESSURES ON BASEMENT WALLS

N. Wagner<sup>(1)</sup>, N. Sitar<sup>(2)</sup>

<sup>(1)</sup> PhD Candidate, Civil & Environmental Engineering, UC Berkeley, USA, [nbwagner@berkeley.edu](mailto:nbwagner@berkeley.edu)

<sup>(2)</sup> Edward G. Cahill & John R. Cahill Professor, Civil & Environmental Engineering, UC Berkeley, USA, [sitar@berkeley.edu](mailto:sitar@berkeley.edu)

## Abstract

Observations of the performance of basement walls and braced retaining structures in recent earthquakes show that failures of basement or deep excavation walls in earthquakes are rare even if the structures were not designed for the actual magnitude of the earthquake loading. For instance, no significant damage or failures of retaining structures occurred in the recent Wenchuan earthquake in China (2008) and the subduction earthquakes in Chile (2010) and Japan (2011). Current design methodologies compute large dynamic loads due to seismic earth pressure that have not been observed in practice. Additionally, while recent research has acknowledged that embedment effects should be incorporated, no specific provisions have been proposed or adopted.

To explore this issue a series of centrifuge scale experiments was carried out with different structures and different types of backfill, as follows: 1) a 6 m deep “stiff” non-displacing cross braced retaining structure; 2) a 6 m deep “flexible” non-displacing cross braced retaining structure and 3) a 13 m deep “stiff” non-displacing basement structure. Comparison of the experimental data to current design methodologies using standard procedures and interpretations (e.g., free field peak ground acceleration as the design acceleration) shows that these are over-conservative and that the depth of embedment is important when dealing with basement structures. Using a seismic coefficient,  $k_{MHEA}$ , corresponding to the maximum depth-averaged acceleration rather than PGA results in better agreement between observed centrifuge data and the computed design load. Numerical analyses using FLAC<sup>2D</sup> corroborate the results.

*Keywords: seismic earth pressure; retaining structure; centrifuge; numerical modeling; embedment effects*

## 1. Introduction

The introduction of more stringent seismic design provisions in recent updates of design codes, e.g. IBC 2015 [1] and FEMA P-750 [2], has increased the demand on seismic design of retaining walls and basement structures and, hence, there is a need for appropriate analysis and design methodology. The most commonly recommended analyses for non-yielding or “rigid” walls (e.g., embedded structures and basement walls) are based on an elastic solution developed by Wood [3]. More recently, Ostadan [4] proposed a simplified method for basement walls that incorporates the characteristics of the ground motion, the backfill, and the embedded structure. The principal problem for a designer is that at high design accelerations, these methods compute very large dynamic forces for non-yielding walls, which appear unrealistic in view of actual experience in recent earthquakes. The experimental and numerical results presented herein show that the previously mentioned analysis methods do not adequately represent the actual seismic demand and that they are indeed conservative, particularly for deeply embedded earth retaining structures.

## 2. Methods of Analysis & Design

The Mononobe-Okabe (M-O) method based on the work of Okabe [5] and Mononobe & Matsuo [6] or the Seed & Whitman [7] simplified method provide a lower bound estimate to the approach proposed by Ostadan [4]. Both methods assume a Coulomb wedge that behaves as a rigid body with no phase

difference between the response of the soil and the structure (Figure 1). These methods are typically used for conventional gravity and cantilever walls, i.e. walls that can deflect, rotate, and translate.

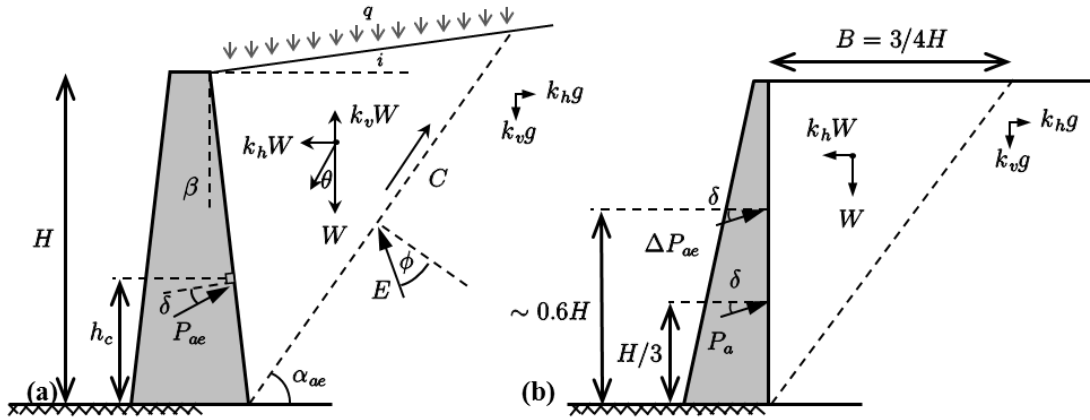


Figure 1: Force diagrams used in (a) modified Okabe [5] and (b) Seed & Whitman [7]

The M-O equation is given by  $P_{ae} = 0.5\gamma H^2(1 - k_v)K_{ae}$ , where  $K_{ae}$  is given by Equation 1,

$$K_{ae} = \frac{\sin(\alpha - \phi + \theta) \cos(\alpha - \beta) \left[ \cos(\beta - i) + \frac{2q}{\gamma H(1 - k_v)} \cos(\beta) \right]}{\cos^2(\beta) \cos(\theta) \sin(\alpha - i) \cos(\alpha - \beta - \phi - \delta)} - \frac{2c}{\gamma H(1 - k_v) \cos(\beta) \sin(\alpha - i) \cos(\alpha - \beta - \phi - \delta)} \quad (1)$$

$\gamma$  is the unit weight of the soil,  $H$  is the height of the wall,  $\phi$  is the angle of internal friction of the soil,  $c$  is the cohesion intercept of the soil,  $\delta$  is the angle of wall friction,  $\beta$  is the slope of the wall relative to the vertical,  $i$  is the slope of the backfill,  $q$  is the surcharge,  $\theta = \tan^{-1}(k_h/(1 - k_v))$ ,  $k_h$  is the horizontal acceleration (in g), and  $k_v$  is the vertical acceleration (in g). The inclusion of cohesion and surcharge follows an update by Prakash & Saran [8]. Increasing cohesion decreases the magnitude of the dynamic load and increases the point of application, while increasing surcharge increases both.

A major limitation of Equation 1 is that it becomes indefinite when  $k_h > \tan \phi + 2c/\gamma H$ . Seed & Whitman [7] sought to remedy this issue by separating the total force on the wall into static and dynamic components as Equation 2

$$P_{ae} = P_a + \Delta P_{ae} = \frac{1}{2}\gamma H^2 K_a + \frac{1}{2}\gamma H^2 \Delta K_{ae} = \frac{1}{2}\gamma H^2 (K_a + \Delta K_{ae}) \quad (2)$$

where  $K_a$  is Coulomb's coefficient of static earth pressure and  $\Delta K_{ae} \approx 0.75k_h$  is the dynamic increment for a vertical wall ( $\beta = 0$ ), horizontal backfill slope ( $i = 0$ ), no surcharge ( $q = 0$ ), and cohesionless backfill ( $\phi = 35^\circ, c = 0$ ). Based on shaking table experiments by Matsuo [9], Seed & Whitman [7] further suggested that the dynamic load increment acts at a height  $0.5H$  to  $0.67H$  above the base of the retaining structure, which led to the so called "inverted triangle" interpretation of dynamic earth pressure. Lastly, Seed & Whitman [7] recommended that 80% of the PGA should be used in seismic design of retaining walls since the peak ground acceleration occurs only for an instant. In addition, the influence of cohesion on the computed seismic coefficient is quite significant and should not be neglected. Specifically, Anderson et al. [10] conclude that the "reduction for typical design situations could be on



the order of about 50 percent to 75 percent”. The good observed seismic performance of retaining structures may be due to the presence of cohesion in typical backfills and in native ground (Sitar et al. [11]).

Mononobe & Matsuo [12] observed that stiffer structures rigidly attached at the base with granular backfill experience higher seismic loads. This problem was first addressed analytically by Wood [3] who modeled linearly elastic soil in a container with rigid walls and a rigid base. The computed dynamic stress increment is zero at the base and maximum at the top of the backfill with the recommended point of application of the resulting force at  $\sim 0.6H$ . The dynamic thrust,  $\Delta P_E$ , for a uniform, constant seismic coefficient  $k_h$  applied throughout the backfill acting on a smooth rigid wall is computed using Equation 3, where Whitman [13] concluded that the value of  $F$  is approximately equal to unity. The Wood [3] solution provides an upper bound estimate to the Ostadan [4] approach, which can be up to 2 to 2.5 times greater than obtained using the M-O method.

$$\Delta P_E = \Delta K_{ae} = F k_h \gamma H^2 \approx k_h \gamma H^2 \quad (3)$$

Ostadan [4] includes the effects of modulus degradation and damping in the backfill by selecting an equivalent seismic coefficient corresponding to the 30% damped spectral acceleration of the ground motion at the natural frequency of the site using the average strain-compatible shear wave velocity profile obtained in a 1D equivalent linear site response analysis. The ground motion is obtained from the site response analysis at the depth of the wall in the free field. This equivalent seismic coefficient is multiplied by the total mass of the backfill (Equation (4)), to determine the dynamic load. The dynamic load is then distributed according to the normalized seismic earth pressure profile in Equation (5, where  $y$  is the normalized height ratio ( $Y/H$ ) measured from the bottom of the wall. Note that FEMA P-750 [2] states “partially embedded structures should not be treated as a non-yielding wall”.

$$m = \rho H^2 / \sqrt{(1 - \nu)(2 - \nu)} \quad (4)$$

$$p(y) = -0.0015 + 5.05y - 15.84y^2 + 28.25y^3 - 24.59y^4 + 8.14y^5 \quad (5)$$

A rigorous analytical solution for a pair of rigid walls with a rigid base with elastic backfill subject to harmonic excitation was presented by Veletsos et al. [14]. For the case of an input frequency of 0 Hz (uniform excitation in the backfill), their solution replicates the solution by Wood [3]. Veletsos & Younan [15], [16], [17] extend the analysis to flexible walls rotationally constrained at the base with a uniform elastic backfill subject to harmonic excitation. They conclude that increasing the relative flexibility of the wall,  $d_w = GH^3/D_w$  (Figure 2a), and base constraint,  $d_\theta = GH^2/R_\theta$  (Figure 2b), decreases the magnitude and point of application of the dynamic load. Veletsos & Younan [16] also conclude that incorporating a backfill shear modulus that increases with depth removes the tensile stresses at the top of the wall (Figure 2c). Younan & Veletsos [18] developed an analytic solution for a flexible wall pinned at the top (representing support conditions of a basement wall) with an elastic backfill subject to harmonic excitation. Again, they concluded that increasing the flexibility of the wall decreases the magnitude of the dynamic load, although the point of application moves up slightly.

Most recently, Kloukinas et al. [19] provide a simplified closed-form solution of Veletsos & Younan [16] by considering a single shape function (i.e., one mode only) for the deformations in the backfill. This allows the governing partial differential equation to be converted into an ordinary differential equation, simplifying the solution at the expense of accuracy; i.e. with increasing frequency of the excitation and base flexibility the contributions of higher modes become more important. The Ostadan [4] solution is essentially the empirical equivalent of the Kloukinas et al. [19] solution with the shape function defined as Equation (5).



#### 4. Numerical Study

In order to evaluate the ability of numerical models to reproduce the experimental results, FLAC<sup>2D</sup> was used to simulate the centrifuge experiment shown in Figure 3 (Wagner & Sitar [25]). The dimensions of the soil domain and the structure were the same as those of the prototype dimensions in the centrifuge experiment. The boundary conditions were specified as a rigid base and the sides of the model were attached to simulate the flexible shear beam container (Figure 4). The total stress soil model UBCHyst (Naesgaard [26]) was used to model the non-linear response of the soil. The shear modulus degradation characteristics of the soil model were calibrated to match Darendeli [27] curves. Input ground motions were the same as those recorded at the base of the centrifuge experiment. The structure elements were attached to the soil grid because interface elements in FLAC<sup>2D</sup> are not well suited to simulate the dynamic earth pressure that was observed in the centrifuge experiment.

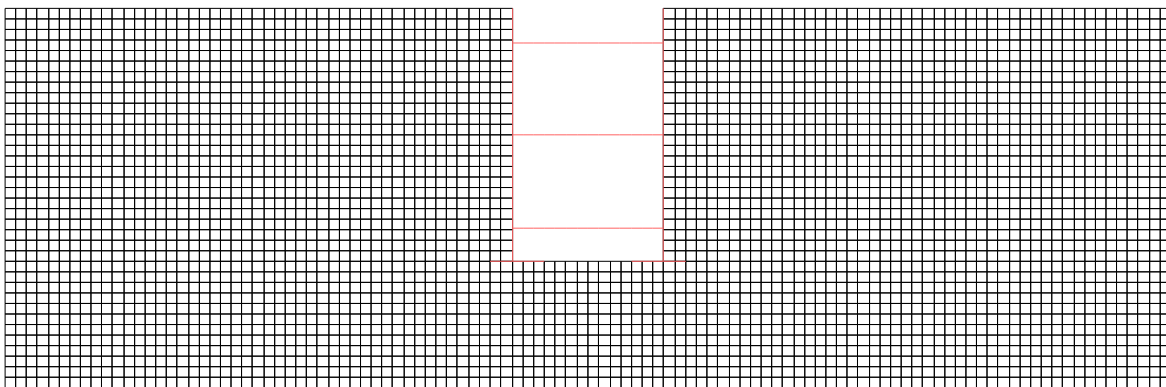


Figure 4: Finite difference mesh developed in FLAC<sup>2D</sup> to simulate Wagner & Sitar [25] experiment

In addition, a series of numerical analyses was performed to simulate the response of four prototype basement structures of varying depth in two different 30 m deep, 120 m wide soil domains (Figure 5). The boundary conditions were specified as a compliant base and free field boundaries on the sides, with radiation damping to approximate 3D effects applied to the entire grid. The structures were 3, 6, 9 and 12 m deep with three 8 m wide bays. The first soil profile corresponded to Site Class D and had the same soil properties from the numerical model of the centrifuge experiment by Wagner & Sitar [25]. The second soil profile corresponded to Site Class C and had shear modulus degradation characteristics calibrated to match Menq [28] curves. Input ground motion records were selected from the PEER database [29] from sites with a similar  $V_{s,30}$  and deconvolved using 1D equivalent linear analysis to 30 m depth. The velocity history from this depth was converted to a shear stress wave history, which was then applied to the compliant base of the model in order to simulate vertically propagating motions (Wagner & Sitar [30]).

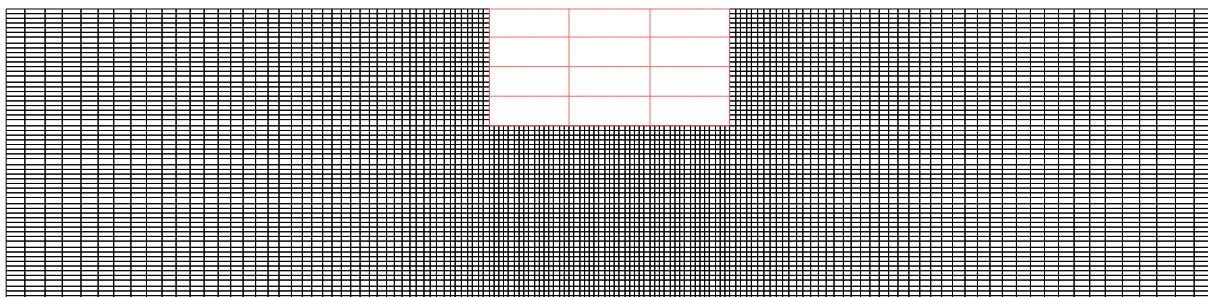


Figure 5: Finite difference mesh of 12 m deep prototype basement structure developed in FLAC<sup>2D</sup>

## 5. Results of the Experimental and Numerical Studies

The dynamic earth pressure in the centrifuge experiment was interpreted by removing the inertial loads from the recordings of the load cells and distributing the load using tributary areas. The pressure in the numerical simulation was interpreted using the axial loads computed in the beam elements as a proxy for the load cells. Additionally, the dynamic earth pressure distribution was computed directly from the horizontal stresses in the soil grid adjacent to the structure. An example plot showing the experimental and computed instantaneous dynamic earth pressure distributions corresponding to the maximum dynamic earth pressure increment ( $\Delta K_{ae}$ ) is shown in Figure 6. The dynamic earth pressure distribution computed by the M-O method is computed using a seismic coefficient,  $k_{MHEA}$ , corresponding to the maximum averaged acceleration over the depth of embedment of the basement (Equation (6)). This is equivalent to  $MHEA/g$  for a uniform backfill, as defined by Bray et al. [31]. The dynamic earth pressure distribution computed by the Seed & Whitman [7] method is computed using 80% of the peak ground acceleration at the surface. The distribution of static at-rest earth pressure is also shown. Note that the pressure increases approximately linearly with depth up to 0.2-0.3 H from the surface and then decreases to zero at the base of the wall for the pressure interpreted from load cells and computed axial loads on the cross struts. In comparison, the computed pressure distribution interpreted from the soil grid in the numerical simulation is more uniform with essentially zero pressure at the surface and at the base of the wall.

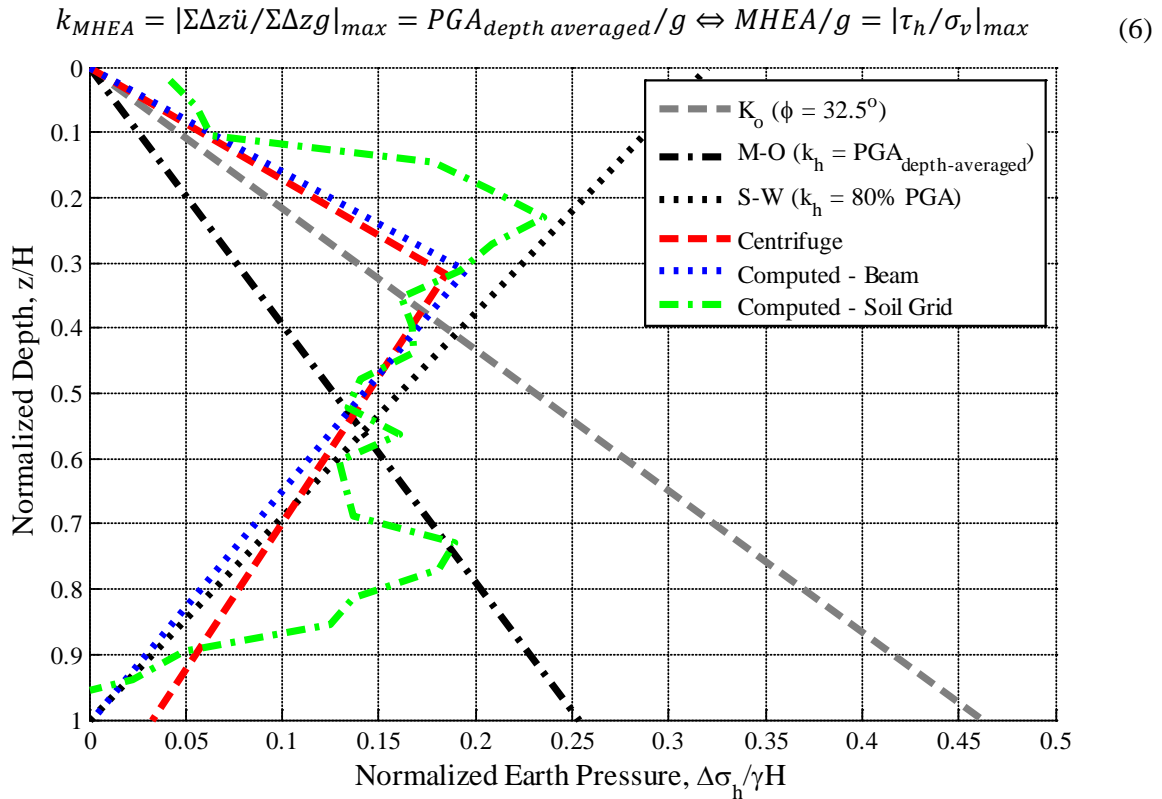


Figure 6: Measured and computed normalized dynamic earth pressure distributions at maximum and minimum  $\Delta K_{ae}$  during Kobe TAK 090-3 for centrifuge experiment and numerical simulation

A set of plots of computed instantaneous dynamic earth pressure distributions throughout the time history in the numerical simulations is presented in Figure 7. The blue lines are the instantaneous pressure distributions corresponding to the maximum computed  $\Delta K_{ae}$ . The equivalent seismic earth pressure

increments computed using the M-O and Seed & Whitman [7] methods, as well as the static at-rest earth pressure, are also shown for reference. As can be seen, the dynamic pressure distribution at maximum  $\Delta K_{ae}$  for the 3 and 6 m tall structures can be reasonably approximated by a triangular distribution, which matches the results obtained by Mikola & Sitar [21] and Candia & Sitar [23]. In contrast, the dynamic pressure distribution at maximum  $\Delta K_{ae}$  for the 9 and 12 m tall structures is essentially uniform with depth, which matches the results of the numerical modeling of the centrifuge experiment by Wagner & Sitar [30]. Note that the pressure is essentially zero at the top and base of the wall, as observed in the numerical modeling of the centrifuge experiment.

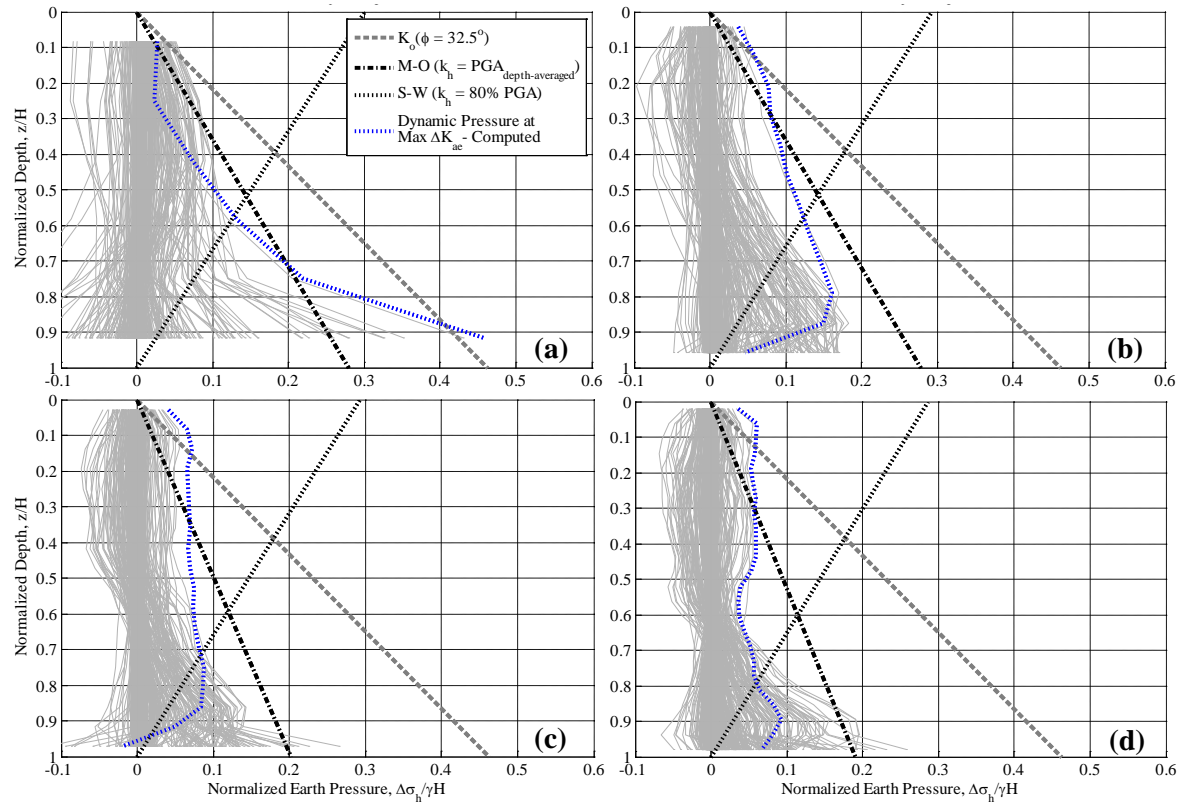


Figure 7 : Computed normalized dynamic earth pressure distributions at maximum and minimum  $\Delta K_{ae}$  during Loma Prieta CAP000 for (a) 3 m basement (b) 6 m basement (c) 9 m basement (d) 12 m basement

These results can be presented as a plot of the dynamic increment of earth pressure,  $\Delta K_{ae}$ , versus the seismic coefficient computed in the numerical model and obtained in the experiments (Figure 8). Analytical solutions by Okabe [5], Seed & Whitman [7], and Wood [3] are also shown for reference. The results from the numerical model reflect the trend of increasing dynamic earth pressure with increasing seismic coefficient. This data show that numerical models can reproduce the results of a centrifuge experiments when the models are properly calibrated with realistic soil behavior. Additionally, using an average measure of acceleration over the depth of the embedded structure seems more appropriate than a single measure from the surface or at the depth of the structure. As can be seen, there is a good agreement between the observed and computed dynamic load compared to the dynamic load computed using the Okabe [5] and Seed & Whitman [7] methods for  $k_{MHEA} \lesssim 0.4$  and for deep structures.

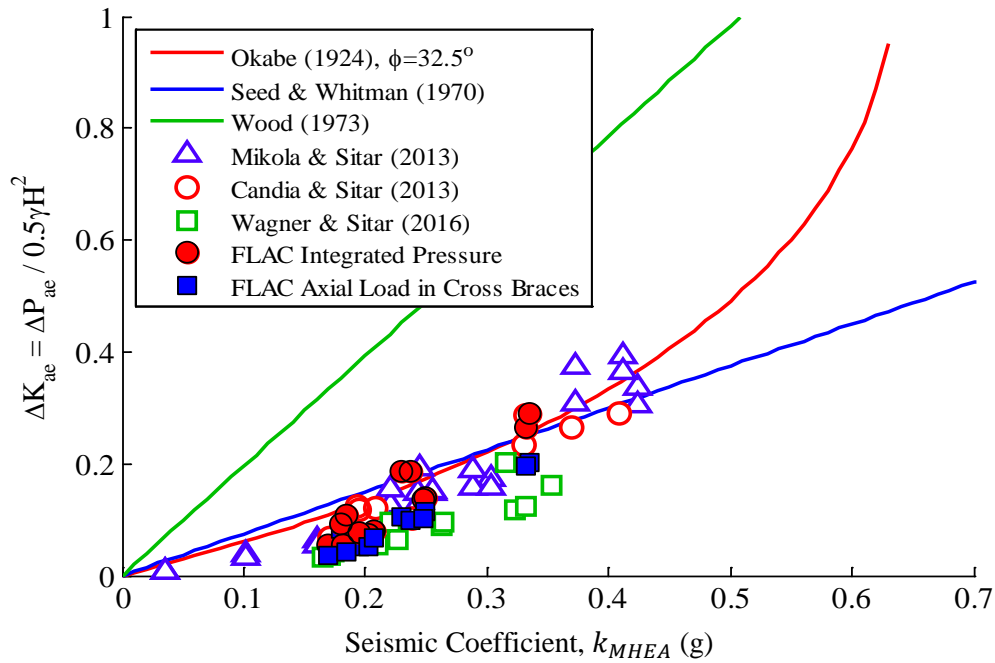


Figure 8: Computed and observed coefficient of dynamic earth pressure increment versus seismic coefficient,  $k_{MHEA}$

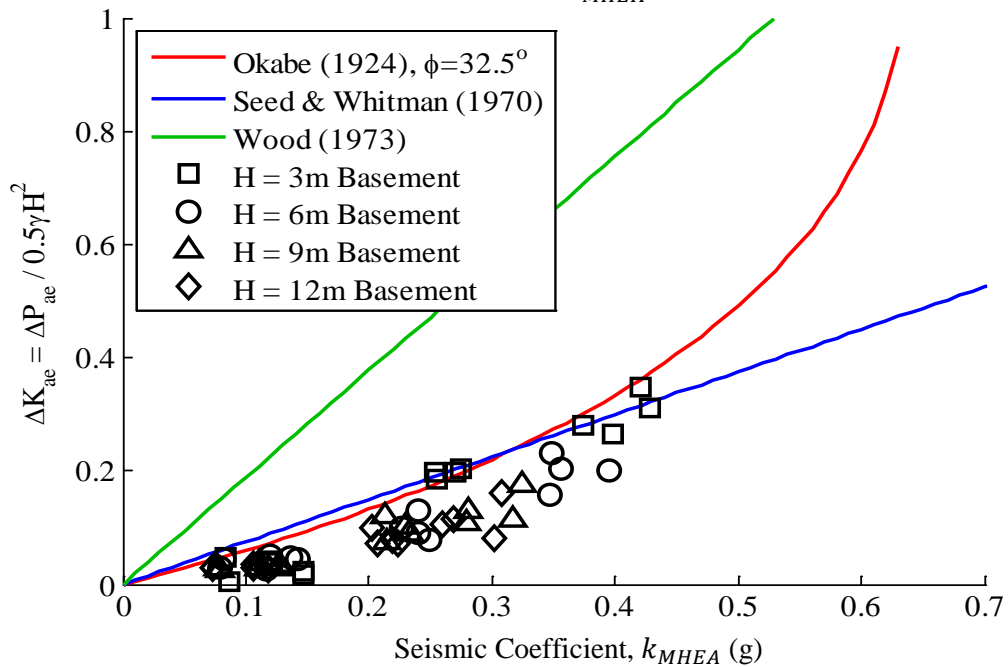


Figure 9: Computed coefficient of dynamic earth pressure increment versus seismic coefficient,  $k_{MHEA}$ , for three-bay, prototype basement structures, Site Class D

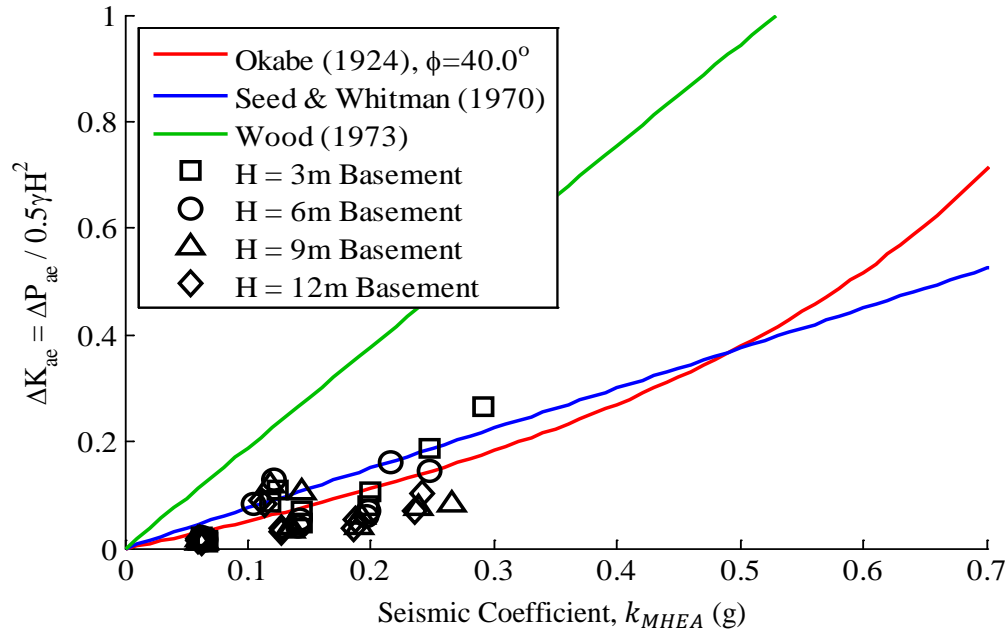


Figure 10: Computed coefficient of dynamic earth pressure increment versus seismic coefficient,  $k_{MHEA}$ , for three-bay, prototype basement structures, Site Class C

The dynamic increment of earth pressure versus the seismic coefficient computed in the numerical models is compared with analytic solutions (Okabe [5]; Seed & Whitman [7]; Wood [3]) for the soft (Site Class D) and stiff (Site Class C) profiles in Figure 9 and Figure 10, respectively. Again, the results from the numerical model match the trend of increasing dynamic earth pressure with increasing equivalent seismic coefficient. Note that the seismic coefficient and the corresponding dynamic increment of earth pressure both decrease with increasing depth of embedment.

The issue of the influence of the height or depth of a retaining structure has been recognized by Anderson et al. [10] who proposed the use of height-dependent seismic design coefficients ( $\alpha$ ) in the M-O method, as shown in Figure 11. As shown on the plot, the results of the centrifuge tests tend to cluster around the lower bound (LB) of the scaling factor defined as  $\alpha = 1 + 0.01H[(0.5\beta) - 1]$ , where  $\beta$  is a measure of the long period (low frequency) intensity of the input ground motion and is 0.5 for the lower bound (LB).

Finally, the difference in the shape of the computed pressure distributions for the shorter (3 and 6 m) and taller (9 and 12 m) prototype basement structures shown in Figure 7 can be assessed by considering the relative stiffness between the structure and the backfill and between the base rotation and the backfill. First, the effective lateral stiffness of the basement structures ( $k_{lat}$ ) can be computed using a simple frame model and static condensation. Then, the relative flexibility of the structures can be computed by modifying the formula by Veletsos & Younan [17] as  $d_w = G_{avg}/k_{lat}$ , where  $G_{avg}$  is the average shear modulus in the backfill over the depth of embedment of the structure. For the softer soil profile (Site Class D),  $d_w$  varies from 0.21 for the 3 m tall structure to 0.65 for the 12 m tall structure. For the stiffer soil profile (Site Class C),  $d_w$  varies from 2.27 for the 3 m tall structure to 4.30 for the 12 m tall structure. The relative stiffness of the base constraint is difficult to assess quantitatively, but a qualitative assessment suggests that  $d_\theta$  is higher (more flexible) for the shorter structures and lower (more rigid) for the taller structures. The competing effects of increasing flexibility of the structure with increasing depth while the base constraint flexibility decreases with increasing depth can be assessed using the dynamic

pressure distributions from Veletsos & Younan [16], [17] in Figure 2. Additionally, Jung & Bobet [32] performed a parametric study to assess the effects of the relative stiffness of a retaining structure and the base constraint on the pressure distribution. They conclude that the wall flexibility has a large effect on the magnitude and distribution of the pressure, whereas the base rotation has a large effect on the magnitude of the pressure and a modest effect on the distribution. The results of the numerical analyses presented herein are consistent with those conclusions.

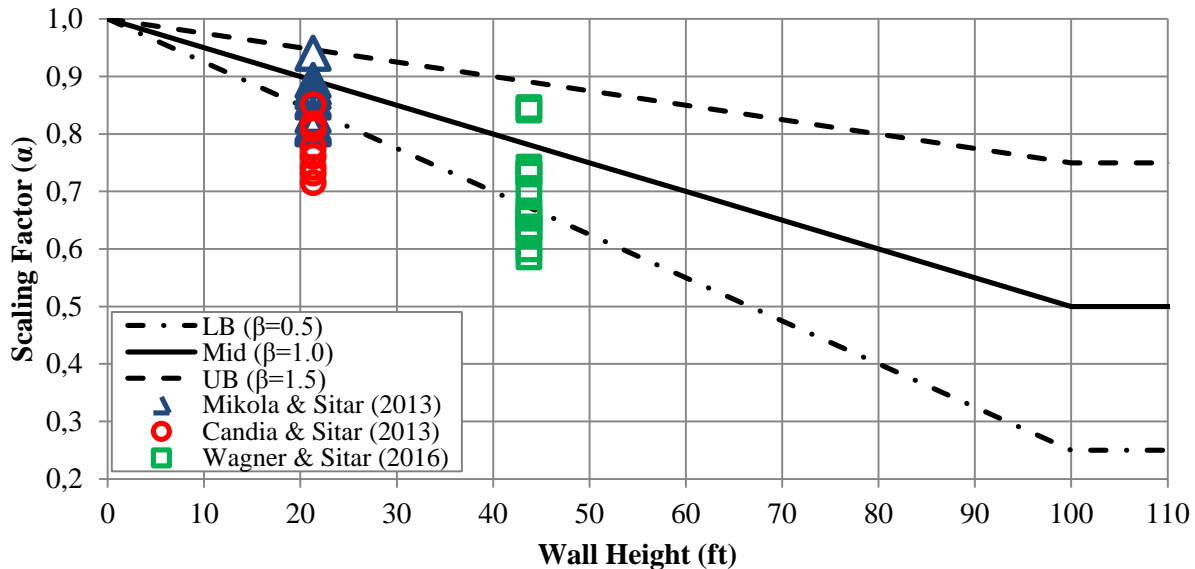


Figure 11: Anderson et al. [10] and experimental height-dependent reduction factor versus wall height

Finally, note that sliding deformation of the retaining structure relative to the soil foundation was not assessed in Veletsos & Younan [15], [16], [17], which also neglects the ability of a shorter basement wall to move together with the backfill and soil foundation. Similar to the case of static earth pressure, the translation of the wall together with the surrounding soil results in approximately triangular distribution of the dynamic earth pressure increment. This is consistent with the dynamic earth pressure distribution computed in the numerical analyses of the short basement walls and observed by Mikola & Sitar [21] and Candia & Sitar [23].

## 6. Conclusions

The results of dynamic centrifuge experiments show that the traditionally used M-O and Seed & Whitman [7] methods of analysis provide a reasonable average estimate for computing seismic loads on retaining structures provided a depth-averaged acceleration measure,  $k_{MHEA}$ , is used as the seismic coefficient. On the other hand, there is no evidence to support the further use of the Wood [3] solution and its derivatives. The results also show that seismic earth pressures increase only moderately with depth (if at all) and are a small fraction of the static pressure at depth for deep basement structures. Further, the seismic earth pressure distributions assumed in the M-O and Seed & Whitman [7] methods do not match the observed distribution for deep basement structures, as observed in the centrifuge experiment and the numerical simulations thereof. Numerical models of prototype structures of various heights show that the seismic earth pressure distribution depends on the depth of embedment, the relative stiffness of the structure and the backfill, and the base rotation constraint.

In addition, the selection of the acceleration measure is critical in computing realistic seismic loads on tall retaining structures and deep basement walls. Typically, the peak acceleration at the surface



or some empirically established fraction thereof has been used as the design acceleration. This is a reasonable design choice for shorter (<6.5 m high) retaining structures, as the phase lag between the top and bottom of the structure is essentially negligible. However, for taller or deeper walls the differences in the phase and amplification of the motion from the base of the structure to the surface can significantly deviate from the assumptions in traditional analyses. For these structures the depth averaged measure of horizontal acceleration,  $k_{MHEA}$ , is more consistent with the experimental and numerical simulation results. Therefore, its use is recommended for the design of tall retaining walls and deep embedded structures.

## 7. Acknowledgements

The funding for this research was provided in part by a grant from the California Geotechnical Engineering Association (CalGeo), the State of California Department of Transportation (Caltrans) Contract No. 65N2170, NSF-NEES-CR Grant No. CMMI-0936376: Seismic Earth Pressures on Retaining Structures, the US Nuclear Regulatory Commission (USNRC) and the Edward G. Cahill and John R. Cahill Endowed Chair Fund.

## 8. References

- [1] International Code Council. (2014): International Existing Building Code, ICC, Country Club Hills, Illinois.
- [2] Building Seismic Safety Council. (2009): NEHRP Recommended Seismic Provisions for New Buildings and Other Structures (FEMA P-750), 2009 Edition. BSSC, Washington, DC.
- [3] Wood, J.H. (1973): Earthquake-Induced Soil Pressures on Structures. *Report EERL 73-05*, Earthquake Engineering Research Laboratory, California Institute of Technology, Pasadena, CA.
- [4] Ostadan, F. (2005): Seismic Soil Pressure for Building Walls – an Updated Approach. *Proceedings of the 11<sup>th</sup> International Conference on Soil Dynamics and Earthquake Engineering and 3<sup>rd</sup> International Conference on Earthquake Geotechnical Engineering*, University of California, Berkeley, 2004.
- [5] Okabe, S. (1924): General theory of earth pressure and seismic stability of retaining wall and dam. *Journal of the Japanese Society of Civil Engineers*, **10** (6), 1277-1323.
- [6] Mononobe, N., Matsuo, H. (1929): On the determination of earth pressure during earthquakes. *Proceedings of the World Engineering Conference*, **9**, 179-187.
- [7] Seed, H.B., Whitman, R.V. (1970): Design of Earth Retaining Structures for Dynamic Loads. *ASCE Specialty Conference, Lateral Stresses in the Ground and Design of Earth Retaining Structures*. Cornell University, Ithaca, New York, 103-147.
- [8] Prakash, S., Saran, S. (1966): Static and dynamic earth pressures behind retaining walls. *Proceedings of the Third Symposium on Earthquake Engineering*. University of Roorkee, Roorkee, India, **1**, 277-288.
- [9] Matsuo, H. (1941): Experimental study on the distribution of earth pressures acting on a vertical wall during earthquakes. *Journal of the Japanese Society of Civil Engineers*, **27** (2).
- [10] Anderson, D.G., Martin, G.R., Lam, I., Wang, J.N. (2008): Seismic Analysis and Design of Retaining Walls, Buried Structures, Slopes, and Embankments (*NCHRP Report 611*). Transportation Research Board, Washington, DC.
- [11] Sitar, N., Mikola, R.G., Candia, G. (2012): Seismically induced lateral earth pressures on retaining structures and basement walls. Keynote Lecture, Geotechnical Engineering State of the Art and Practice, *Keynote Lectures from GeoCongress 2012*, GSP 226, ASCE, 2012.
- [12] Mononobe, N., Matsuo, H. (1932): Experimental Investigation of Lateral Earth Pressure during Earthquakes. *Earthquake Research Institute and Research Institute of Public Works, Department of Home Affairs*, Japan.



- [13] Whitman, R.V. (1991): Seismic Design of Earth Retaining Structures. *Proceedings, Second International Conference on Recent Advances in Geotechnical Earthquake Engineering and Soil Dynamics*, St. Louis, Missouri, 1767-1778.
- [14] Veletsos, A.S., Parikh, V.H., Younan, A.H. (1995): Dynamic response of a pair of walls retaining a viscoelastic solid. *Earthquake Engineering and Structural Dynamics*, **24** (12), 1567-1589.
- [15] Veletsos, A.S., Younan, A.H. (1994a): Dynamic Soil Pressures on Rigid Vertical Walls. *Earthquake Engineering and Structural Dynamics*. **23** (3), 275-301.
- [16] Veletsos, A.S., Younan, A.H. (1994b): Dynamic Modeling and Response of Soil-Wall Systems. *Journal of Geotechnical Engineering*. **120** (12), 2155-2179.
- [17] Veletsos, A.S., Younan, A.H. (1997): Dynamic response of cantilever retaining wall. *Journal of Geotechnical and Geoenvironmental Engineering*. **123** (2), 161-172.
- [18] Younan, A.H., Veletsos, A.S. (2000): Dynamic response of flexible retaining walls. *Earthquake Engineering and Structural Dynamics*, **29** , 1815-1844.
- [19] Kloukinas, P., Langousis, M., Mylonakis, G. (2012): Simple Wave Solution for Seismic Earth Pressures on Nonyielding Walls. *Journal of Geotechnical and Geoenvironmental Engineering*, ASCE, **138** (12), 1514-1519.
- [20] Clough, G.W., Fragaszy, R.J. (1977): A Study of Earth Loadings on Floodway Retaining Structures in the 1971 San Fernando Valley Earthquake. *Proceedings, 6<sup>th</sup> World Conference on Earthquake Engineering*. **3**, 2455-2460.
- [21] Mikola, R.G., Sitar, N. (2013): Seismic earth pressures on retaining structures in cohesionless soils. *Report No. UCB GT 13-01*, March 2013, p. 217.
- [22] Mikola, R.G., Candia, G., Sitar, N. (2013): Seismic earth pressures on braced wall in sand (ROOZ01). *Network for Earthquake Engineering Simulation* (distributor), Dataset, DOI: 10.4231/D3HD7NS4P
- [23] Candia, G., Sitar, N. (2013): Seismic Earth Pressures on Retaining Structures in Cohesive Soils. *Report No. UCB GT 13-02*, August 2013, p. 161.
- [24] Candia, G., Mikola, R.G., Sitar, N. (2013): Seismic earth pressures on braced wall and displacing retaining wall in clay (GC01). *Network for Earthquake Engineering Simulation* (database), Dataset, DOI: 10.4231/D37W67572
- [25] Wagner, N., Sitar, N. (2013): Seismic earth pressures in a deep basement wall on dry sand (NW01). *Network for Earthquake Engineering Simulation* (distributor), Dataset, DOI: 10.4231/D3D21RJ44
- [26] Naesgaard, E. (2011): A hybrid effective stress – total stress procedure for analyzing soil embankments subjected to potential liquefaction and flow. Ph.D. thesis, University of British Columbia, Vancouver, Canada.
- [27] Darendeli, M. (2001): Development of a new family of normalized moduli reduction and material damping curves. Ph.D. thesis, University of Texas at Austin.
- [28] Menq, F. (2003): Dynamic Properties of Sandy and Gravelly Soils. Ph.D. thesis, University of Texas at Austin.
- [29] PEER Ground Motion Database. Accessed on April 15, 2015. <<http://ngawest2.berkeley.edu/>>
- [30] Wagner, N. Sitar, N. (2016): Seismic Earth Pressure on Basement Walls with Cohesionless Backfill. *Report No. UCB GT 16-02*, May 2016.
- [31] Bray, J.D., Rathje, E.M., Augello, A.J., Merry, S.M. (1998). Simplified seismic design procedures for geosynthetic-lined, solid waste landfills, *Geosynthetics International*, **5** (1-2), 203-235.
- [32] Jung, C., Bobet, A. (2008): Seismic Earth Pressures Behind Retaining Walls: Effects of Rigid-body Motions, *Proceedings of Geotechnical Earthquake Engineering and Soil Dynamics IV*, D. Zeng, M. Manzari & D. Hiltunen, eds., ASCE, Sacramento, CA.